Soft Matter

Non-destructive determination of functionalized polyelectrolyte placement in layer-by-layer films by IR ellipsometry

Journal:	*Soft Matter*
Manuscript ID	SM-ART-08-2021-001246.R1
Article Type:	Paper
Date Submitted by the Author:	26-Oct-2021
Complete List of Authors:	Cho, Szu-Hao; University of Akron, Polymer Engineering Lewis, Elizabeth; University of Akron, Polymer Engineering Zacharia, Nicole; University of Akron, Polymer Engineering Vogt, Bryan; Penn State University Park, Chemical Engineering Engineering

ARTICLE

Non-destructive determination of functionalized polyelectrolyte placement in layer-by-layer films by IR ellipsometry

Received 00th January 20xx,
Accepted 00th January 20xx

DOI: 10.1039/x0xx00000x

Szu-Hao Cho,[a, †] Elizabeth A. Lewis, [a,†] Nicole S. Zacharia[a*] and Bryan D. Vogt[b,*]

Layer-by-layer (LbL) assembly facilitates controlled coatings on a variety of surfaces with the ability to manipulate the composition through the film thickness through the selection of the complementary pairs. However, the characterization of the composition profiles tends to be destructive and require significant compositional differences that can limit their utility. Here, we demonstrate the ability to non-destructively quantify the depth dependence of the allyl content associated with the selective incorporation of poly(sodium acrylate-co-allylacrylamide) (84:16 mol:mol) (allyl-PAA) in LbL films based on the assembly of poly(diallyldimethylammonium chloride) (PDAC)/poly(acrylic acid) (PAA) and PDAC/allyl-PAA. Although the atomic composition of the film is not dramatically influenced by the change between PAA and allyl-PAA, the absorption in the IR near 1645 cm^{-1} by the allyl group provides sufficient optical contrast to distinguish the LbL components with spectroscopic ellipsometry. The use of IR spectroscopic ellipsometry can determine the thickness of layers that contain allyl-PAA and alo gradients that develop due to re-arrangements during the LbL process. With multiple films fabricated simultaneously, the location of the gradient between the 1st and 2nd series of multilayers (e.g., first PDAC/PAA bilayers and then PDAC/allyl-PAA bilayers) can be readily assess. The results from a variety of different multilayer architectures indicate that the gradient is located within the thickness expected for the 1st deposited bilayer stack (PDAC/PAA or PDAC/allyl-PAA). These results are indicative of a dynamic dissolution-deposition process (in- and out- diffusion) during the fabrication of these LbL films. These results provide additional evidence into the mechanisms for exponentially growth in LbL assemblies. The ability to quantify a gradient with the low contrast system examined indicates that spectroscopic IR ellipsometry should be able to non-destructively determine compositional gradients for most polymer films where compositional gradients exist.

Introduction

Increasing demands on the properties exhibited by polymer coatings for a wide variety of applications from automotive[1] to marine[2] to healthcare[3] industries tend to necessitate multiple distinct layers to provide the requisite functionality due to differing requirements at interfaces. For example, the chemistries associated with enhanced adhesion/corrosion resistance and non-wetting surface coatings tend to be orthogonal, so multiple different materials are needed; commonly, these materials can be applied as pre-treatment and then the primary coating. The multiple coating layers can lead to interdiffusion of components depending on the solvents used and compatibility of the components.[1] The interfacial characteristics can define the performance of the coating in these cases. More recently, interfacial segregation of multiple components in a single coating has been designed to produce self-stratified coatings to decrease application costs, but their efficacy is tied directly to the efficiency of the stratification.[4, 5] For biomedical applications, coatings that release therapeutic agents tend to also include additional functional requirements, such as antifouling or extended release, which can be addressed through the incorporation of multiple layers in the coating.[6, 7] The ability to precisely place functionality spatially through the thickness of coatings is important for a wide range of applications, but it can be challenging to measure the location within the coatings depending on the resolution desired.

Many of the measurements developed to assess the spatial distribution through the thickness of coatings are destructive. For thick multiple layer coatings, microtome sectioning with FTIR characterization has been used to determine the interfacial composition, but this method tends to offer limited resolution (>1 μm) and is destructive.[1] Similar cross-sections have been

[a.] Department of Polymer Engineering, University of Akron, Akron, OH 44325
[b.] Department of Chemical Engineering, The Pennsylvania State University, University Park, PA 16802.
† Authors contributed equally to this work.
* To whom correspondence should be addressed: bdv5051@psu.edu (B.D.V.), nzach1@gmail.com (N.S.Z.)
Electronic Supplementary Information (ESI) available: ^{1}H NMR, LbL growth kinetics, fit extinction coefficients for the base LbL films, and fits of ellipsometric angles with comparisons between models. See DOI: 10.1039/x0xx00000x

characterized with confocal Raman spectroscopy to provide improved spatial resolution.[8] Both Raman and FTIR rely on differences in the spectra between components due to chemical bonding differences. When the mechanical properties of the components are distinct, nanoindentation on the cross-sections can provide information about the layered structure.[8] Controlled etching along with x-ray photoelectron spectroscopy (XPS) provides higher resolution (~ 10 nm) for the depth dependent composition if the etching is uniform for the components and does not damage the polymer to lead to loss of functionality being tracked by XPS.[9] The bonding differences between the components must also be clearly resolved through the binding energies involved, commonly from a heteroatom present in only one component.[9] Non-destructive methods with high resolution include x-ray reflectivity, but the contrast depends on the electron density difference which is commonly small for polymers.[10] Neutron reflectivity provides the potential for enhanced resolution of the interface through selective deuteration, but this adds significant expense.[11] Moreover, relatively sharp interfaces (typically order of 10 nm or less for the interfacial width)[12] are required to accurately resolve the interfacial width with reflectivity,[13] which can be challenging for industrially relevant multi-layered coatings where the interfaces can commonly be 100's of nm.[1]

Layer-by-layer (LBL) assembly through entropic liberation of counterions[14-16] or through controlled covalent reactions[17-19] provide a facile route to precisely tune the chemistry locally within a polymer coating. The ability to selectively alter the chemistry through the thickness of the film provides extreme control over the functionality.[20] These LBL films provide model materials with controlled chemistry spatially through the thickness of the coating as confirmed by neutron reflectivity.[21] However, the precision in the spatial distribution of the chemistry can be challenged for exponentially growing LBL assemblies due to chain diffusion during assembly that drives the accelerated growth.[22, 23] This blurring of the interfaces could adversely impact performance, but characterization of these broader interfaces can be challenging.[9] This challenge in direct characterization has led to some controversy in the literature about the exact mechanisms associated with exponential growth during LBL deposition. From fluorescence measurements, there appears to be both diffusion of chains into the interior of the film as well as diffusion out to the surface to promote complexation.[24] This in-out diffusion has been postulated as a key component to the exponential growth, but other work has suggested that outward dissolution of chains is not necessary to model the exponential growth[25] and the diffusion of associative sites is dominant, not chain diffusion.[26] Selective deuteration has been able to demonstrate some dissolution of polyelectrolyte complexes during deposition of linearly growing LBL films,[27] but the broader interfaces that develop with exponential growth lead to dampening of the Kessig fringes and loss of sensitivity to quantify the interfaces in these materials. More recently, there has been some evidence for loss of polyelectrolytes during the deposition from ATR-FTIR, but this was unable to provide any insights into the length scales over which dissolution occurs and this dissolution was attributed to only the outmost polyelectrolytes.[28] The sensitivity to unequivocally assess if diffusion of polyelectrolytes out that results in dissolution occurs during deposition for exponential growth requires a length scale intermediate to fluorescence (microns) and neutron reflectivity (10's of nm for interfacial width).

Beyond these fundamental questions about the mechanism of growth in LBL films, there are additional cases where enhancements in the characterization of films with small differences in chemistry would be useful. Added functionality desired for some applications can also influence the morphology of the coating; for example, ionomers within LBL assemblies provide hydrophobicity, which has been exploited for wetting, but also lead to rough surfaces that would be detrimental for optical applications.[29] With advances in click chemistry,[30] post-deposition modification[31] provides an approach to add functionality without significantly changing assembly by LBL. This approach has been demonstrated to stabilize and functionalize LBL assemblies.[32] However, the initial functionalization of the polymer for the click reactivity (e.g., -ene, -yne) challenges many methodologies developed for characterization of multilayer films. The electron and neutron scattering length densities of most polymers will not be dramatically altered by a small fraction of these functional groups, while addition of hydrocarbons only will limit the quantitative characterization by XPS.

Here we demonstrate the potential of spectroscopic ellipsometry in the infrared (IRSE) to characterize the distribution of functionalized polymers within LBL films. A common polyelectrolyte pair of poly(diallyldimethylammonium chloride), PDAC, and poly(acrylic acid), PAA, was examined for the base material. Allyl functionalized (16.3 mol%) PAA (allyl-PAA) was selectively substituted for the PAA at different locations in the LBL film. The presence of the allyl functionality provides the source of contrast in the IR due to its absorption near 1645 cm^{-1}, while the resolution of the composition through the thickness is enabled by the sensitivity of ellipsometry to the complex dielectric constant as a function of depth. For these LBL films that contain both PAA and allyl-PAA, the ellipsometric data require multiple layers in order to obtain an adequate fit. The overall thicknesses from these fits are consistent with the kinetic growth curves for the allyl-PAA/PDAC and PAA/PDAC bilayers. However, these ellipsometric data provide new insights into exponential growth of these LBL films as the location of the diffuse interface between allyl-PAA/PDAC and PAA/PDAC bilayers is closer to the substrate than expected. These results indicate that the out diffusion postulated in the mechanism of exponential LBL growth[24] is not fully captured with complexation at the interface, but results in the dissolution of some of the previously deposited polymers. These measurements demonstrate the potential for IRSE to resolve the distribution of polymer components through the thickness of the film even when the differences in optical properties are small.

Experimental

Materials.

Poly(diallyldimethylammonium chloride) solution (PDAC, nominal M_w = 400,000-500,000 g/mol, 20 wt% in H_2O), allylamine (≥99%), N,N'-dicyclohexylcarbodiimide (DCC, 99%), 1-methyl-2-pyrrolidinone (NMP, 99%), deuterium oxide (D_2O, 99.9 atom % D), sodium chloride (NaCl, ≥99.0%), sodium hydroxide (NaOH), and hydrochloric acid (HCl, 37%) were obtained from Sigma-Aldrich. Poly(acrylic acid) (PAA, nominal M_w = 50,000 g/mol, 25 wt% aqueous solution) was purchased from Polysciences (Warrington, PA). Methanol, sulfuric acid (H_2SO_4, 98%), and hydrogen peroxide (35% w/w in H_2O, Cat No. BDH7814-3) were obtained from VWR International. All chemicals were used as received. Deionized (DI) water was produced from a Milli-Q DQ-3 system (Millipore, Bedford, MA, USA) with a resistivity of 18.2 MΩ·cm.

Synthesis of allyl-PAA.

PAA was amidized by allylamine in NMP solution. PAA (1.0 g) was dissolved in NMP (50 mL) in a 100 mL three-neck flask fitted with a magnetic stir bar, condenser and nitrogen atmosphere and stirred at 57 °C for 8 h to fully dissolve the polymer. Allylamine (0.176 g, 3.08 x 10^{-4} mol) was added rapidly to the flask, followed byDCC (0.828 g, 4.01 x 10^{-3} mol) in NMP (5 mL). The solution was allowed to react at 57 °C for 24 h. The reaction was terminated by placing the mixture in an ice after 24 h. Concentrated sodium hydroxide solution (10 M, 30 mL) was added dropwise to precipitate the allyl-PAA. The mixture was allowed to stand for 30 min for the precipitated allyl-PAA to sediment. The precipitated polymer was separated from the supernatant and then washed with 60 °C NMP and subsequently cold methanol. The polymer product was collected by centrifugation and dried in oven (60 °C) overnight. The polymer was then dissolved in DI water and reprecipitated in methanol. The product was obtained by centrifugation and dried in oven (60 °C) overnight. The collected polymer was ground into powder and dried in vacuum. The allyl functional group composition was quantified by ^{1}H NMR spectroscopy. As determined from NMR (Figure S1), the acrylic acid on the polymer was modified to allyl on 16.3 mol % of the AA repeat units.

Fabrication of LbL films.

Solutions of PDAC, PAA and allyl-PAA were prepared in DI water. The chemical structures of these polyelectrolytes are shown in Figure 1a. The PDAC solution was prepared at 30 mM with respect to the repeat unit with NaCl added to produce ionic strength of 0.2 M. The ionic strength of the water rinse solution was adjusted to 0.2 M with NaCl. PAA or allyl-PAA solutions were prepared at 40 mM with respect to the carboxylic acid groups present. The pH of PAA and allyl-PAA solutions were adjusted to 4.5 with 1 M HCl or 1 M NaOH solutions with no added NaCl.

Double side polished and highly doped silicon wafers (150 µm thick, 5-10 ohm·cm) were obtained from University Wafer and used for the IR ellipsometric measurements. The wafers were cleaned with freshly prepared piranha solutions (mixture of 98% sulfuric acid and 35% hydrogen peroxide at v/v = 7/3) for 2 h at room temperature and then rinsed with excess DI water to remove any residual piranha solution. The substrates were dried by air flow and then treated with air plasma for 5 min immediately before the layer by layer (LbL) assembly of the polyelectrolyte multilayers.[33-35] The cleaned silicon wafers were used for the sequential deposition of polycation (PDAC) and polyanion (PAA or allyl-PAA) at room temperature using a StratoSequence VI dipper (NanoStrata Inc., USA). The clean substrates were first immersed into PDAC solution for 5 min followed by three DI water rinse baths for 1 min each. Subsequently, the substrates were immersed into PAA or allyl-PAA solution for 5 min, followed by three DI water rinse baths for 1 min each. This cycle was repeated until the desired number of bilayers, *x*, were obtained, where the film nomenclature for the single pair films are $(PDAC/PAA)_x$ and $(PDAC/allyl\text{-}PAA)_x$. In cases of mixed LbL films, the same nomenclature is used with the layers listed in order from the substrate to the surface such that allyl-PAA in the layer near the substrate would be denoted as $[(PDAC/allyl\text{-}PAA)_a/(PDAC/PAA)_b]$, where the subscripts *a* and *b* represent the number of bilayers of each sublayer. After LbL assembly, the multilayer films were dried at 60 °C for 12 h prior to characterization.

Characterization.

Nuclear Magnetic Resonance (NMR) Spectroscopy

^{1}H NMR (Varian Mercury 300 MHz spectrometer) was used to quantify the allyl functionalization of the allyl-PAA. The allyl-PAA samples for NMR analysis were prepared by dissolving the polymer in D_2O at 2 wt%. The NMR measurements were performed with 3 s relaxation time and 32 transients for each sample.

Fourier Transform Infrared Spectroscopy (FTIR)

The chemistry of the PDAC/PAA and PDAC/allyl-PAA LbL films were characterized with FTIR (Thermos Scientific Nicolet iS50). The measurements were performed in transmission mode through double side polished silicon wafers (150 µm thick, 5-10 ohm·cm). A resolution of 2 cm^{-1} and 64 scans were used for each sample. The clean, uncoated silicon wafer was used as the background for these FTIR measurements.

Ellipsometry

A UV-Vis/Near IR spectroscopic ellipsometer (J.A. Woollam, M-2000UI) was used to elucidate the film thickness and optical constants between 243 nm to 1680 nm for the LbL films using a recursive fitting protocol. The ellipsometric angles were fit using previously reported silicon wafer stack (silicon, interdiffusion layer, and silicon oxide)[36] and a Cauchy layer to describe the LbL coating as the optical constants over this wavelength range are

essentially unchanged with the allyl functionality. Due to the lack of contrast in the UV-Vis/NIR, only the overall film thickness was determined using this ellipsometer.

To assess the compositional differences in the films, an IR-Vase ellipsometer (J.A. Woollam, Mark II) was used to obtain the ellipsometric angles in the IR region (3330 cm^{-1} to 590 cm^{-1}). In the IR region, the optical constants for the silicon are highly dependent on the doping, so each silicon substrate was measured prior to LbL coating. The ellipsometric angles measured for the silicon wafer were fit using a genosc layer with Gaussian peak and Kramers-Kronig oscillators to describe the absorption in the IR by the silicon. The $(PDAC/PAA)_x$ and $(PDAC/allyl\text{-}PAA)_x$ films on silicon substrates, were used to obtain the optical constants in the IR by using the thickness of the film from the UV-Vis-NIR measurements. The optical constants were fit to the genosc model, where the absorption in the IR was described by Gaussian and Lorentzian oscillators. These material optical constants were used to fit the ellipsometric angles for the more complex LbL films that contain both PDAC/PAA and PDAC/allyl-PAA. These fits provided the thicknesses of the PDAC/PAA and PDAC/allyl-PAA layers within the film as well as compositional gradients.

For the complex LbL film stacks, e.g. PDAC/PAA on PDAC/allyl-PAA, the process for fitting the IR ellipsometric data began with the film thickness determined from UV-Vis/NIR ellipsometry. The thickness of the film after each sublayer deposition was measured with UV-Vis/NIR ellipsometry on an analogous LBL film that was deposited at the same time as the full stack with the slide stainer to provide insight into the expected structure of the films. The IR-SE data for the full stack were then fit with a variety of models to determine the sensitivity of the measurement to the small change in the chemistry of the films associated with the allyl functionalization. These include a single layer model using the same general oscillator model described above, distinct layers of PDAC/PAA and PDAC/allyl-PAA using the material optical constants developed from the $(PDAC/PAA)_x$ and $(PDAC/allyl\text{-}PAA)_x$ films, and graded interfaces between the PDAC/PAA and PDAC/allyl-PAA using the same optical constants. The gradient was modeled using a graded intermix layer (containing 21 distinct layers for the model fit) where the shape of the gradient was defined by the thickness of the intermix layer and the exponent associated with the mathematical description of the gradient. The overall film thickness was within 30 nm for the two ellipsometric measurements in all cases examined.

Results and discussion

Figure 1b illustrates schematically the protocol associated with the LBL deposition of the polycation and polyanion on the silicon substrate. Initially, the clean silicon wafer is exposed to PDAC solution and the PDAC adsorbs to the negatively charged hydrated native silicon oxide. Three washes in 0.2 M aqueous NaCl remove weakly adsorbed PDAC, but the surface remains positively charged to promote the irreversible adsorption of either PAA or allyl-PAA. Subsequent washes remove weakly adsorbed polyanion to produce a bilayer containing polycation/polyanion. This sequential process is then repeated to build up films of desired thickness. Figure S2 illustrates the growth in film thickness associated with the number of PDAC/PAA and PDAC/allyl-PAA bilayers. The growth profile for PDAC/PAA, according to literature,[37, 38] can be varied depending on the degree of interaction between the two assembled polyelectrolytes. For the deposition conditions used for the assembly of PDAC/PAA, linear growth is observed as expected.[37, 38] The allyl functionalization increases the observed film growth rate, but also appears to change the growth from linear to exponential.[24, 39] The transition from linear to exponential growth may be explained by the decreasing intermolecular interactions between PDAC and allyl-PAA due to the steric hinderance of allyl functional groups, which enables more chain diffusion during the LbL process.

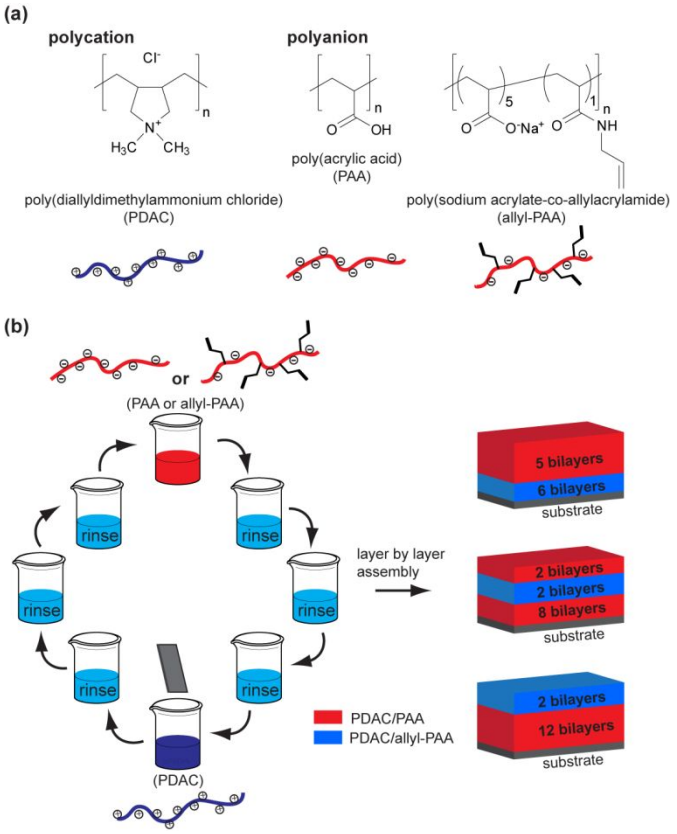

Figure 1. (a) Chemical structure of the three different polymers used to fabricate the LbL films (b) Schematic of the LbL process.

Beyond the deposition of simple bilayer films of PDAC/PAA or PDAC/ally-PAA, the polyanion can be changed after a specified number of bilayers to produce architectures where the location of the allyl functionality can be tuned. This stratified structure relies on the preservation of the bilayer structure, which does not necessarily occur especially for exponentially growing films where exchange/diffusion through the film thickness drives the accelerated growth.[9] Thus, when the allyl-PAA in bilayers are deposited near the substrate, in the middle of the film and at the surface may led to differences in the stratification as the

growth mechanism (linear vs. exponential) depends on the bilayer pair. These measurements will provide insights into how well the stratified structure can be maintained in these allyl functionalized polymers that can be readily modified through click chemistry.

To understand if IR ellipsometry can be used to differentiate between allyl-PAA and PAA bilayers in the films, it is instructive to first examine the contrast in the system. Generally, contrast for ellipsometry is related to the complex dielectric constant for the materials within the measured wavelength range. For typical ellipsometers operating in the visible region, the contrast between most polymers tends to be small due to the lack of distinct absorption bands within this region and the general similarities in the refractive index, typically near 1.5. With insufficient contrast, ellipsometric characterization of multiple layers of polymers within a film tends to provide only the average optical properties and the overall film thickness without clear insights into the compositional differences within the film. An advantage of ellipsometric measurements of polymers within the IR region is the ability to distinguish between polymers due to the change in refractive indices near absorption peaks as required by Kramers-Kronig relations.[40] Thus most polymer pairs can be distinguished with IR ellipsometry. Here, the contrast is limited as the only difference is 10% of the PAA that is modified with the allyl functionality.

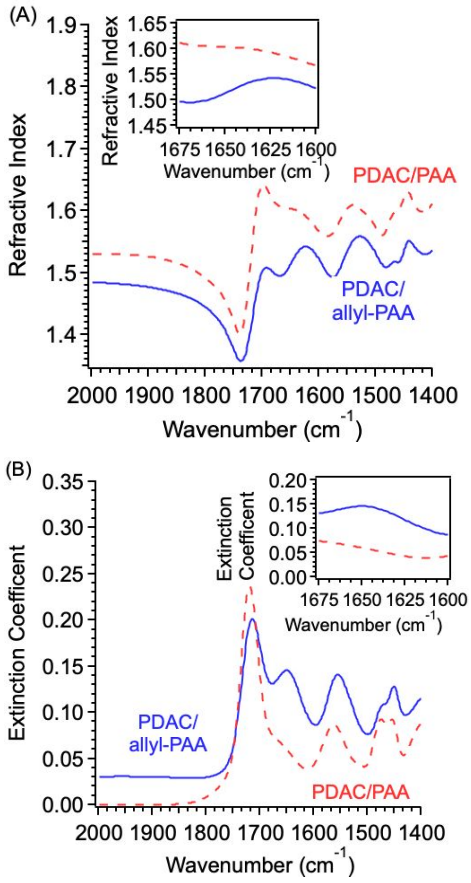

Figure 2. Comparison of the optical constants, (A) refractive index and (B) extinction coefficient, obtained from fits of the IR VASE data for 495 nm $(PDAC/PAA)_{17}$ and 643 nm $(PDAC/allyl\text{-}PAA)_9$ films. The insets illustrate the differences near the absorption peak from the allyl group (1645 cm^{-1}).

Figure 2 illustrates the refractive index and extinction coefficient determined from the best fits of ellipsometric data in the IR for films of PDAC/PAA and PDAC/allyl-PAA. As the only difference in the chemistry of these films should be the 16.3% mol of allyl units, the optical constants appear similar except near 1650 cm^{-1} where the absorption of the allyl group occurs. Figure S3 illustrates the best fits of the ellipsometric angles and the associated residual. The fits are excellent with residuals less than 1º over the full wavelength range. The extinction coefficients obtained from the Gaussian oscillators in these fits (Figure 2B) were compared with transmission FTIR absorption spectra as shown in Figure S4. There is good agreement between these spectra in terms of the relative absorption and peak position for PDAC/PAA and PDAC/allyl-PAA films, which provides confidence in the fits of the ellipsometric data.

To assess if the limited contrast shown in Figure 2 is sufficient to elucidate compositional differences through the thickness, initially 12 bilayers of PDAC/PAA were deposited and then 2 bilayers of PDAC/ally-PAA. Figure 3A and 3B illustrates the ellipsometric angles obtained from IR SE for this film. These angles cannot be fit adequately by using the optical properties obtained for the pure PDAC/PAA or PDAC/allyl-PAA as shown in Figure S5. Features in the angles in the wavenumber range between 1700-1600 cm^{-1} are not resolved in these cases. Significant improvements in the fits are obtained when considering the stratification of the PDAC/PAA and PDAC/allyl-PAA layers as shown in Figure 3.

The compositional profile from this best fit is illustrated in Figure 3C with reasonable stratification of the layers. From the fit, the interfacial width between the PDAC/PAA and PDAC/allyl-PAA is approximately 58 nm, which is broader than can typically be resolved by x-ray or neutron reflectivity.[41] The diffusion of the allyl-PAA into the previously deposited PDAC/PAA layers is clearly evident when comparing the ideal profile obtained from the thickness after completion of the PDAC/PAA bilayer stack. This ideal profile is determined from additional LBL films that were fabricated at the same time as the multilayer stacks shown in Figure 3. The thickness of the PDAC/PAA was determined by stopping the deposition of one sample after 12 bilayers and removing this film prior to PDAC/allyl-PAA deposition. The PDAC/PAA and PDAC/allyl-PAA stack was fabricated in one step without drying to avoid artifacts that could occur on drying between deposition steps. Although the gradient appears to be symmetric from the best fit, the location of the gradient within the film appears to be fully within the region where the initially deposited PDAC/PAA should be present. As the thickness of the deposited bilayers is highly controllable (Figure S2), this difference in the amount of the PDAC/PAA deposited shown in Figure 3 suggests that some of the initially deposited PAA has been removed (dissolved) and replaced with allyl-PAA. This result suggests some dissolution of the polyelectrolytes from the film during the deposition stage.

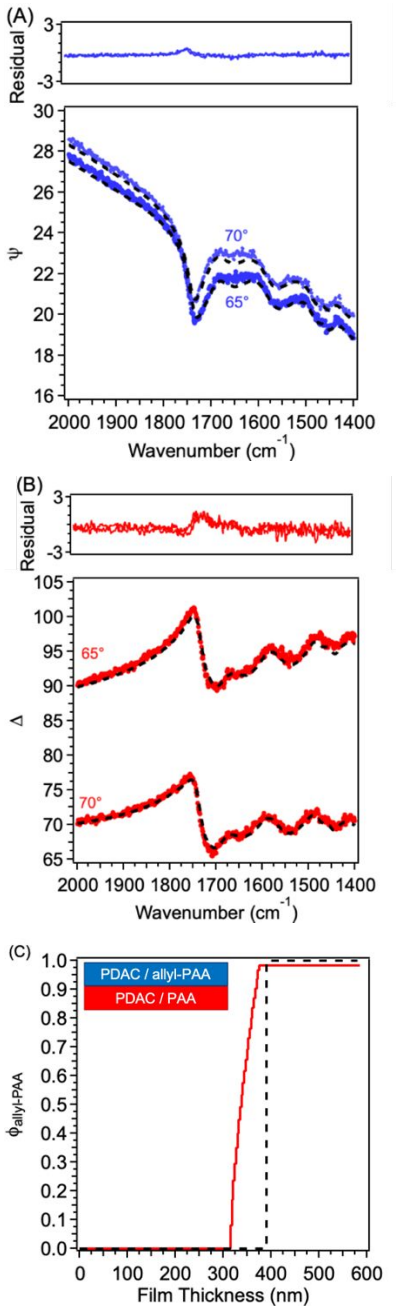

Figure 3. Ellipsometric angles (Ψ, Δ) for (A,B) (PDAC/allyl-PAA)$_2$ on (PDAC/PAA)$_{12}$ with fits to a bilayer model with a graded interface. (C) Depth profile showing the composition of the film. The volume fractions are relative to the PDAC/allyl-PAA bilayer optical constants. The black dashed line is the ideal profile based on the growth kinetics of the PDAC/allyl-PAA films and PDAC/PAA films. The substrate is at zero thickness.

Partial dissolution of some of the complex during deposition has been argued against based on no mass or thickness loss ever observed during deposition.[25] However, the adsorption and complexation from solution is a dynamic event that relies on the preferential adsorption of polyelectrolytes to build the film thickness. These IR ellipsometry measurements indicate that some of the previously deposited PAA dissolves but the film growth increases with additional layers, which requires the adsorption from solution to be significantly more favourable than dissolution. This would lead to an increased mass or thickness observed from *in-situ* time dependent measurements, such as with QCM,[42-44] SPR,[42] and/or ellipsometry.[43] Measurements of the refractive index of the film near a waveguide substrate has demonstrated a clear shift in the composition even when the film is considerably thicker than the lengthscale probed.[44] Similarly, ATR-FTIR measurements have provided evidence of the release of some polyelectrolytes during deposition associated with exponential growth.[28] The results here suggest that the top 50-75 nm of the film is removed during subsequent depositions. The growth of PDAC/allyl-PAA behaves similar to exponentially growing LbL films (Figure S2) and this also leads to a relatively broad gradient due to interdiffusion[9] in addition to the partial dissolution during growth. This gradient is approximately 70 nm wide, which is far greater than can be resolved with neutron reflectivity. It should be noted that the depth of the depletion of the underlying layer and the interfacial profile are likely dependent on a plethora of process variables (ionic strength, pH, thickness, dipping time, molecular mass, etc).

To better understand the behaviour of these similar bilayers, an analogous film was fabricated, but with PDAC/allyl-PAA at the substrate and then PDAC/PAA deposited on top of this layer. Figure 4A illustrates the composition profile obtained from then best fits of the ellipsometric angles (Figure S6). The interface of this profile is considerably sharper (Figure 4A) than the films with the order of the layers reversed (Figure 3C). There is a small foot on the interface with the allyl-PAA appearing to slightly diffuse into the PDAC/PAA during its deposition. However, the stratification of the functional LBL bilayers is significantly improved in this conformation, but the location of the gradient is again within the 1st layer based on the measurement of the film after completing the PDAC/allyl-PAA layer. These results can be rationalized in terms of the growth mechanisms. PDAC/PAA appears to grow linearly (Figure S2), so stratification would be expected.[9, 15, 23] The surface dissolution of some previously deposited materials has been recently quantified with isotopic labelling and neutron reflectivity, which is consistent with the determined profile.[27] However, the thinner initial bottom PDAC/allyl-PAA layer could also influence the profile due to potential for enhanced adsorption to the substrate[45] that limits the kinetics of the exchange of polyelectrolytes.

To confirm the sharper interface is not a result of the order of the deposition in these LbL films, a hybrid film with the allyl-PAA in the center of the film was examined with IR spectroscopic ellipsometry as shown in Figure S7. Figure 4B illustrates the compositional profile associated with the best fit of the ellipsometric angles. The stratification of the deposited layers is clearly evident in the film, but the location of the functionalized LbL layer is offset from the individual growth curves, similar to the other films examined. These profiles are all consistent with some dissolution of previously deposited polymers during the LBL fabrication. Additionally, the interfacial width is sharper for the bottom of the PDAC/allyl-PAA layer than the top. In

comparing with the other geometries, the interfacial width between PDAC/allyl-PAA and PDAC/PAA layers appears to be correlated with the location in the film. As the substrate is approached, the width is more narrow and then increases as the interface moves away from the substrate. This result is consistent with reduced mobility of the polymer chains in the LbL film by their interactions with the substrate (silicon oxide). The reduction in the interdiffusion as the substrate is approached is consistent with prior reports in the literature for confined polymer films.[46, 47] These IR ellipsometric measurements confirm the stratification of the LbL structure overall, but also illustrate more details about the complex growth mechanism associated with exponential growth that appears to include adsorption, diffusion, and dissolution during the growth cycles.

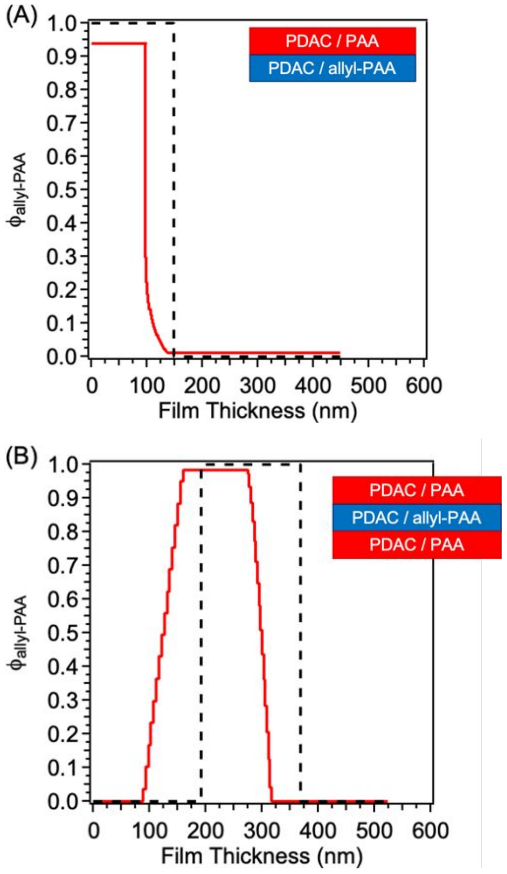

Figure 4. Depth profile showing the composition determined from fits of the ellipsometric angles to a model with (A) bilayer with graded interface for $(PDAC/PAA)_5$ on $(PDAC/allyl-PAA)_6$ and (B) trilayer with graded interfaces for $(PDAC/PAA)_2$ on $(PDAC/allyl-PAA)_2$ on $(PDAC/PAA)_8$. The black dashed lines are the ideal profile based on the growth kinetics of the PDAC/allyl-PAA films and PDAC/PAA films based on the deposition schedule utilized.

To better illustrate this point, Figure 5 presents a direct comparison in the overall thickness determined after each sublayer deposition measured in the UV-vis/Near IR wavelength range (243nm – 1680nm) with the profile obtained from a single measurement in the IR range (3330 cm^{-1} to 590 cm^{-1}). For the UV-vis/NIR measurements, the overall thickness of the film was measured after each set of deposition cycles for a given bilayer system in an analogous sample such that the deposition conditions were identical (from multiple samples prepared at the same time) to the overall stack measured with IR ellipsometry. For the trilayer comparison, three samples were prepared in parallel. One sample was removed after completion of the first PDAC/PAA deposition to determine the bottom layer in Figure 5 by UV-Vis/NIR ellipsometry. After completion of the PDAC/allyl-PAA layer, one additional sample was removed to determine the thickness after the deposition of the PDAC/PAA and PDAC/allyl-PAA layers. Finally, the stack was completed with a capping layer of PDAC/PAA and this sample was measured by both UV-Vis/NIR ellipsometry to obtain the total thickness and by IR ellipsometry to obtain the overall thickness and the compositional profile through the thickness of the film. In Figure 5, the difference between the prior thickness and the total thickness after subsequent deposition as measured by UV-Vis/NIR ellipsometry was assumed to be the film thickness of newly deposited layer. Comparing the thicknesses between the ellipsometric measurements for the three film geometries, the overall film thickness is similar, but the lower layer thicknesses are smaller from the IR measurements than expected based on the analogous layer alone. These results indicate some dissolution of the underlying allyl-PAA and PAA in addition to the intermixing of the PDAC/allyl-PAA and PDAC/PAA bilayers during LBL deposition.

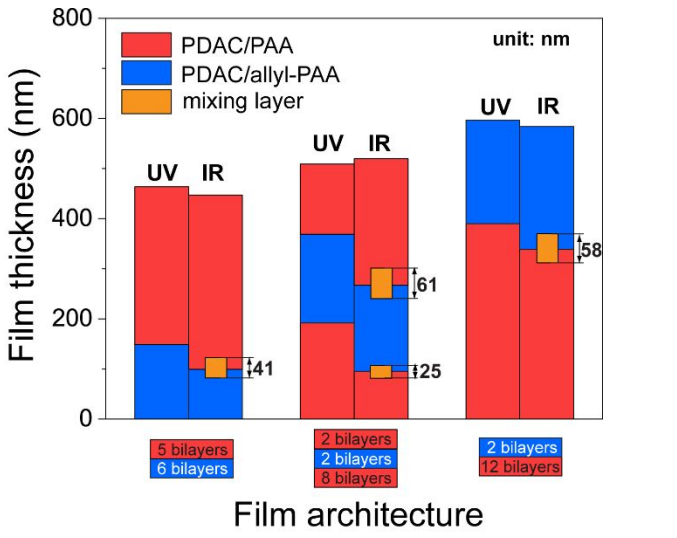

Figure 5. Comparison of sublayer thicknesses determined from UV-Vis/NIR (UV) and IR ellipsometry for 3 film architectures examined.

These measurements provide additional insights into the in- and out- diffusion of polymer chains during LBL deposition, but the exact profile will depend on the deposition conditions and polymer characteristics. The molecular mass of the polyelectrolyte will influence the mobility, especially within the associating LBL film, and thus the time required to diffuse. The relevant timescale should be proportional to the ratio of the square of the depth into the film where polymer is removed and the diffusion coefficient of the polyelectrolyte chains, analogous to the argument by Fares and Schlenoff on time scale for site diffusion to achieve exponential growth.[26] If we consider

the midpoint of the gradient in the composition between the PDAC/PAA and PDAC/allyl-PAA layers as a reference point to calculate the diffusion length for the dissolution of chains, the effective diffusivity (D_{eff}) can be estimated as:

$$D_{eff} \approx \frac{l^2}{2t}$$

where *l* is the difference in the lower layer thickness between UV-Vis/NIR ellipsometry measurements on the removed film and IR ellipsometry of the stack and *t* is the deposition time for a layer (5 min). Examination of the four interfaces leads to D_{eff} ranging between 1.5 x 10^{-13} to 4.3 x 10^{-14} cm^2/s. These values are within the range that has been attributed to site diffusion, not polymer chain diffusion.[26] This suggests that there may be additional mechanisms at play that enable dissolution of chains during LBL deposition. As the growth kinetic varied significantly between PDAC/PAA and PDAC/allyl-PAA, this system is likely not the best to sort of these details with IR ellipsometry. The shift in the IR from selective deuteration[26] can lead to larger changes in the absorption spectra than with the allyl functionalization of the PAA shown here. We hypothesize that the use of deuterated vs. protonated near monodisperse polyelectrolytes with the same molecular mass would provide an ideal environment to probe in- and out- diffusion along with dissolution in LBL films, where IR ellipsometry provides the ability to measure thicker films and more diffuse interfaces than is possible with neutron reflectivity, which has been more commonly applied to these systems.[27, 48-51] These systems should enable clear insights into the factors that control the extent and the length scales associated with dissolution of previously deposited polyelectrolytes during the buildup of LBL films.

Conclusions

Here, we demonstrate the utility of spectroscopic ellipsometry in the IR to elucidate compositional profiles through the thickness of polymer films. The ability to distinguish limited chemical contrast by IR was tested using layer-by-layer assembled of polyelectrolytes, where poly(diallyldimethylammonium chloride) (PDAC) was assembled with either poly(acrylic acid) (PAA) or poly(sodium acrylate-co-allylacrylamide) (84:16 m:m) (allyl-PAA). The only difference between these polymers was the 16.3 mol% allyl group, which should provide limited contrast for XPS depth profiling given the low concentration of N in the allyl PAA relative to that in PDAC that is present in all layers. However, the allyl group provides absorption in the IR that is isolated from other functional groups in the LbL films. This absorption associated with the allyl group provides sufficient contrast for statistically significant differences in recursive fits of the ellipsometric angles to produce compositional profiles through the thickness of the films. Three different architectures (PDAC/PAA on PDAC/allyl-PAA; PDAC/allyl-PAA on PDAC/PAA; and PDAC/PAA on PDAC/allyl-PAA on PDAC/PAA) were examined. The layer-by-layer approach enabled the total thickness of the film after each layer deposition to be assessed with standard UV-vis/NIR ellipsometry. The best fits of the ellipsometric angles in the IR produced compositionally graded profile that demonstrated some dissolution of the materials during growth from intermediate measurements from each bilayer set, but also provided insights into the gradients that developed during the deposition. These measurements provide evidence for out diffusion and some partial dissolution of prior deposited materials during LBL growth. These non-destructive measurements with IR spectroscopic ellipsometry demonstrated the potential to assess limited compositional gradients through the thickness of polymer films, which could be useful for a variety of applications in coatings.

Conflicts of interest

There are no conflicts to declare.

Acknowledgements

This work was partially supported by the National Science Foundation under grant numbers CMMI-1462284 and DMR-1425187.

Notes and references

1. K. Adamsons, *Prog. Org. Coat.*, 2002, **45**, 69-81.
2. A. Rosenhahna, T. Ederth and M. E. Pettitt, *Biointerphases*, 2008, **3**, IR1-IR5.
3. M. R. Abidian and D. C. Martin, *Adv. Funct. Mater.*, 2009, **19**, 573-585.
4. D. J. Walbridge, *Prog. Org. Coat.*, 1996, **28**, 155-159.
5. A. Beaugendre, S. Degoutin, S. Bellayer, C. Pierlot, S. Duquesne, M. Casetta and M. Jimenez, *Prog. Org. Coat.*, 2017, **110**, 210-241.
6. U. Maver, K. Xhanari, M. Žižek, D. Korte, L. Gradišnik, M. Franko and M. Finšgar, *Eur. J. Pharm. Biopharm.*, 2018, **128**, 230-246.
7. Q. Wei and R. Haag, *Mater. Horiz.* 2015, **2**, 567-577.
8. A. M. Forster, C. A. Michaels, L. Sung and J. Lucas, *ACS Appl. Mater. Interfaces*, 2009, **1**, 597-603.
9. J. B. Gilbert, M. F. Rubner and R. E. Cohen, *Proc. Natl. Acad. Sci. USA*, 2013, **110**, 6651-6656.
10. T. P. Russell, *Mater. Sci. Rep.*, 1990, **5**, 171-271.
11. A. Karim, G. P. Felcher and T. P. Russell, *Macromolecules*, 1994, **27**, 6973-6979.
12. K. Kunz, J. Reiter, A. Goetzelmann and M. Stamm, *Macromolecules*, 1993, **26**, 4316-4323.
13. X. L. Zhou and S. H. Chen, *Phys. Rep.*, 1995, **257**, 223-348.
14. J. Schmitt, T. Gruenewald, G. Decher, P. S. Pershan, K. Kjaer and M. Loesche, *Macromolecules*, 1993, **26**, 7058-7063.
15. K. C. Wood, J. Q. Boedicker, D. M. Lynn and P. T. Hammond, *Langmuir*, 2005, **21**, 1603-1609.
16. G. Decher, M. Eckle, J. Schmitt and B. Struth, *Curr. Opin. Colloid Interface Sci.*, 1998, **3**, 32-39.
17. H.-I. Shao, S. Umemoto, T. Kikutani and N. Okui, *Polymer*, 1997, **38**, 459-462.
18. J.-E. Gu, S. Lee, C. M. Stafford, J. S. Lee, W. Choi, B.-Y. Kim,

K.-Y. Baek, E. P. Chan, J. Y. Chung, J. Bang and J.-H. Lee, *Adv. Mater.,* 2013, **25**, 4778-4782.
19. W. J. Yang, D. Pranantyo, K.-G. Neoh, E.-T. Kang, S. L.-M. Teo and D. Rittschof, *Biomacromolecules*, 2012, **13**, 2769-2780.
20. T. Boudou, T. Crouzier, K. Ren, G. Blin and C. Picart, *Adv. Mater.*, 2010, **22**, 441-467.
21. G. J. Kellogg, A. M. Mayes, W. B. Stockton, M. Ferreira, M. F. Rubner and S. K. Satija, *Langmuir*, 1996, **12**, 5109-5113.
22. P. Lavalle, V. Vivet, N. Jessel, G. Decher, J.-C. Voegel, P. J. Mesini and P. Schaaf, *Macromolecules*, 2004, **37**, 1159-1162.
23. N. S. Zacharia, D. M. DeLongchamp, M. Modestino and P. T. Hammond, *Macromolecules*, 2007, **40**, 1598-1603.
24. C. Picart, J. Mutterer, L. Richert, Y. Luo, G. D. Prestwich, P. Schaaf, J.-C. Voegel and P. Lavalle, *Proc. Natl. Acad. Sci. USA*, 2002, **99**, 12531-12535.
25. P. Lavalle, C. Picart, J. Mutterer, C. Gergely, H. Reiss, J. C. Voegel, B. Senger and P. Schaaf, *J. Phys. Chem. B*, 2004, **108**, 635-648.
26. H. M. Fares and J. B. Schlenoff, *J. Am. Chem. Soc.*, 2017, **139**, 14656-14667.
27. A. Sill, P. Nestler, A. Weltmeyer, M. Passvogel, S. Neuber and C. A. Helm, *Macromolecules*, 2020, **53**, 7107-7118.
28. M. Muller, *Molecules*, 2019, **24**, 2141.
29. H.-c. Huang and N. S. Zacharia, *Langmuir*, 2015, **31**, 714-720.
30. X. Hou, C. Ke and J. Fraser Stoddart, *Chem. Soc. Rev.*, 2016, **45**, 3766-3780.
31. F. Lin, J. K. Zheng, J. Y. Yu, J. J. Zhou and M. L. Becker, *Biomacromolecules*, 2013, **14**, 2857-2865.
32. L. A. Connal, C. R. Kinnane, A. N. Zelikin and F. Caruso, *Chem. Mater.*, 2009, **21**, 576-578.
33. X. Huang, J. D. Chrisman and N. S. Zacharia, *ACS Macro Lett.*, 2013, **2**, 826-829.
34. X. Huang, M. J. Bolen and N. S. Zacharia, *Phys. Chem. Chem. Phys.*, 2014, **16**, 10267-10273.
35. Y. Gu, X. Huang, C. G. Wiener, B. D. Vogt and N. S. Zacharia, *ACS Appl. Mater. Interfaces*, 2015, **7**, 1848-1858.
36. C. M. Herzinger, B. Johs, W. A. McGahan, J. A. Woollam and W. Paulson, *J. Appl. Phys.*, 1998, **83**, 3323-3336.
37. M. Elzbieciak, M. Kolasinska and P. Warszynski, *Colloids Surf. A*, 2008, **321**, 258-261.
38. T. Alonso, J. Irigoyen, J. J. Iturri, I. L. larena and S. E. Moya, *Soft Matter*, 2013, **9**, 1920-1928.
39. J. Borges and J. F. Mano, *Chem. Rev.*, 2014, **114**, 8883-8942.
40. T. Q. Sai, M. Saba, E. R. Dufresne, U. Steiner and B. D. Wilts, *Faraday Discuss.*, 2020, **223**, 136-144.
41. E. K. Lin, W. I. Wu and S. K. Satija, *Macromolecules*, 1997, **30**, 7224-7231.
42. B. Schoeler, E. Poptoschev and F. Caruso, *Macromolecules*, 2003, **36**, 5258-5264.
43. J. J. I. Ramos, S. Stahl, R. P. Richter and S. E. Moya, *Macromolecules*, 2010, **43**, 9063-9070.
44. E. Hubsch, V. Ball, B. Senger, G. Decher, J. C. Voegel and P. Schaaf, *Langmuir*, 2004, **20**, 1980-1985.
45. S. Napolitano, S. Capponi and B. Vanroy, *Eur. Phys. J. E*, 2013, **36**, 61.
46. B. Zuo, H. Zhou, M. J. B. Davis, X. P. Wang and R. D. Priestley, *Phys. Rev. Lett.*, 2019, **122**, 217801.
47. S. J. Li, J. W. Li, M. M. Ding and T. F. Shi, *J. Phys. Chem. B*, 2017, **121**, 1448-1454.
48. H. W. Jomaa and J. B. Schlenoff, *Macromolecules*, 2005, **38**, 8473-8480.
49. R. Steitz, V. Leiner, R. Siebrecht and R. von Klitzing, *Colloids Surf. A,* 2000, **163**, 63-70.
50. A. F. Xie and S. Granick, *Macromolecules*, 2002, **35**, 1805-1813.
51. O. Felix, Z. Q. Zheng, F. Cousin and G. Decher, *Comptes Rendus Chimie*, 2009, **12**, 225-234.